

---

# EYE KNOW YOU: METRIC LEARNING FOR END-TO-END BIOMETRIC AUTHENTICATION USING EYE MOVEMENTS FROM A LONGITUDINAL DATASET

---

A PREPRINT

**Dillon Lohr**

Department of Computer Science  
Texas State University  
San Marcos, TX 78666 USA  
dj170@txstate.edu

**Henry Griffith**

Department of Computer Science  
Texas State University  
San Marcos, TX 78666 USA  
hkgriffith1@gmail.com

**Oleg V Komogortsev**

Department of Computer Science  
Texas State University  
San Marcos, TX 78666 USA  
ok11@txstate.edu

April 22, 2021

## ABSTRACT

While numerous studies have explored eye movement biometrics since the modality’s inception in 2004, the permanence of eye movements remains largely unexplored as most studies utilize datasets collected within a short time frame. This paper presents a convolutional neural network for authenticating users using their eye movements. The network is trained with an established metric learning loss function, multi-similarity loss, which seeks to form a well-clustered embedding space and directly enables the enrollment and authentication of out-of-sample users. Performance measures are computed on GazeBase, a task-diverse and publicly-available dataset collected over a 37-month period. This study includes an exhaustive analysis of the effects of training on various tasks and downsampling from 1000 Hz to several lower sampling rates. Our results reveal that reasonable authentication accuracy may be achieved even during a low-cognitive-load task or at low sampling rates. Moreover, we find that eye movements are quite resilient against template aging after 3 years.

**Keywords** Eye movements, biometric authentication, metric learning, template aging

## 1 Introduction

Eye movement biometrics have received considerable attention in the literature over the past two decades [1]. This focus is motivated by the specificity and permanence of human eye movements [2]. Eye movement biometric systems offer notable advantages over alternative modalities, including the ability to support liveness detection [3, 4] and spoof-resistant continuous authentication [5]. Eye movements are also well suited for integration within multimodal biometric systems [6].

In other biometrics domains (e.g., person re-identification [7], speaker verification [8]), a technique called metric learning (more specifically, deep metric learning) has seen great success. Metric learning aims to embed input data into a well-clustered embedding space, where embeddings from the same class are close together and embeddings from different classes are far apart. This is in contrast to more common classification-based approaches (e.g., training with a softmax classification layer) that do not necessarily enforce such properties on the embedding space. According to one study [9], training with cross-entropy loss is theoretically similar to using pair-based loss functions like triplet loss [7] and multi-similarity loss [10]. Even so, we hypothesize that there may be practical differences between cross-entropy loss and metric learning loss functions, including how well the embedding space is clustered. A survey of the most common metric learning loss functions is given in [11]. Recent studies have also begun considering metric learning for eye movement biometrics [12, 13].

A common limitation in the current eye movement biometrics literature is the formulation of eye movement biometrics as a closed-set problem in which all identities are present during training. This is not very practical for real-world

biometrics applications in which new identities need to be enrolled, authenticated, and identified at prediction time. Additionally, the permanence of eye movements is largely unexplored, as most of the literature trains and evaluates their models on datasets collected within a short time period. Another prevailing limitation is the lack of a unifying dataset. Many studies collect new data for the express purpose of testing their methodology without releasing the data to the public, making it virtually impossible to replicate those studies. Moreover, even for studies that do release their datasets, it is often impossible to determine whether any performance differences between two studies is due to one approach being superior or simply due to the use of different datasets.

The research described herein attempts to address many of the aforementioned limitations while further exploring the application of metric learning for eye movement biometrics. We train a convolutional neural network (CNN) that learns meaningful embeddings via multi-similarity (MS) loss [10]. Inputs consist of fixed-length subsequences of eye movements during various tasks, including reading, tracking jumping dots, watching videos, and playing an interactive game. Similarity scores are produced as the cosine similarity between the centroid embeddings of pairs of recordings. The proposed technique is verified on several tasks from the GazeBase dataset [14], which consists of 322 participants recorded up to 18 times each over a 37-month period. We also compare against a statistical baseline.

The main contributions of this study are:

- The application of metric learning for the domain of eye movement biometrics is further explored using multi-similarity loss, which is an established, modern loss function. Multi-similarity loss should accelerate learning compared to older metric learning loss functions like contrastive loss or triplet loss, and it should lead to better-clustered embedding spaces compared to non-metric-learning loss functions like cross-entropy loss.
- To the best of our knowledge, this study is the first to assess the permanence of eye movements with as much as 37 months separating the recordings used for enrollment and verification.
- To the best of our knowledge, this is the most task-diverse and sampling rate-diverse study to date, as it explores 6 different tasks and 5 different sampling rates. There is a common belief in the literature that high-cognitive-load tasks (e.g., reading [15] or visual search [16]) are necessary to achieve the best authentication performance, but our findings reveal that a low-cognitive-load task in the form of a simple back-and-forth jumping dot may result in a similar level of authentication performance.

## 2 Prior Work

Since the introduction of eye movements as biometrics in 2004 [17], significant research has focused on improving their viability. A collective review of related work published prior to 2015 may be found in [18]. Moreover, comparative results for studies analyzing common datasets are provided in [19], which summarizes the results of the most recent BioEye competition. As noted within these reviews, the majority of prior work uses a common processing pipeline, with the recordings initially partitioned into specific eye movement events using a classification algorithm, followed by the formation of the biometric template as a vector of discrete features from each event. One problem with such approaches is that event classification is a difficult problem [20], so it adds another layer of complexity that influences biometric performance. Only recently have studies begun utilizing deep learning models [21] or metric learning [12].

The winners of the BioEye 2015 competition, George & Routray [22], used a radial basis function (RBF) network for computing similarities between probe and gallery vectors. Features describing the position, velocity, and acceleration for fixations and saccades were extracted from the segmented signal. The algorithm was validated using a dataset of 153 individuals recorded twice during both a reading task (TEX) and a random saccades task (RAN) with 30 minutes between recording sessions and recorded again after one year. They achieved an equal error rate (EER) of 2.59% for RAN and 3.78% for TEX when the recording sessions were separated by 30 minutes. When the recording sessions were separated by one year, they achieved 10.96% EER for RAN and 9.36% for TEX. As the proposed method requires retraining the network upon the enrollment of each new user, it is not feasible for large-scale practical deployment.

In addition to eye movement-specific features, other representations of eye movement recordings have also been explored in the literature. For example, Li et al. [16] used a multi-channel Gabor wavelet transform (GWT) to extract texture features from eye movement trajectories during a visual search task. Support vector machine (SVM) classifiers were used for biometric identification and verification. Results were verified using a data set consisting of 58 subjects recorded across several trials, with a minimum EER of 0.89% reported. Texture-based eye movement features were recently reinvestigated in [23], where downsampling of the filtered images was proposed for the feature extraction step in order to preserve spatial structure. In addition to the aforementioned restriction regarding new user enrollment, both of these studies utilized recordings with only a small temporal separation.

Jia et al. [21] introduced deep learning techniques for eye movement biometrics. A recurrent neural network (RNN) was built using long short-term memory (LSTM) cells. The output layer used softmax to produce class probabilities.

Table 1: A summary of the methodological aspects of selected works. ST means short-term and LT means long-term.  
 \*: dataset was previously public but is unavailable at the time of writing.  
 \*\*: a modified version or subset of the dataset is publicly available.

Study	Year	Open-set?	Tasks	Sampling rates (Hz)	N subjects	Test-retest interval	Public dataset?
[17]	2004	N	Jumping dot	250	9	same day	N
[22]	2015	N	Reading; jumping dot	250	153 (ST); 37 (LT)	30 min. (ST); 1 year (LT)	N*
[24]	2017	Y	Reading	1000	298 (ST); 68 (LT)	med. 19 min. (ST); med. 11.1 months (LT)	Y** [14]
[16]	2018	N	Visual search	300, 150, 75, 30	58	same day (ST); avg. 18 days (LT)	N
[21]	2018	N	Image viewing	500	32	≤ 30 min.	N
[12]	2019	Y	Video viewing	30	210	same day	Y [27]
[28]	2020	Y	Reading (ST); jumping dot (LT)	1000	62 (ST); 10 (LT)	same day (ST); 2–8 weeks (LT)	Y** [28]
[4]	2020	Y	Jumping dot	1000	150	≥ 1–4 weeks	Y [4]
[13]	2020	Y	Reading	1000	269	avg. 20 min.	Y** [14]
Present	2021	Y	Reading; jumping dot; static dot; video viewing; interactive game	1000 (all tasks); 500, 250, 125, 31.25 (reading only)	322	20 min. to 37 months	Y [14]

Their approach was validated using a dataset of 32 subjects recorded across several trials of a high-cognitive-load task, with a minimum EER of 0.85% reported. This study did not explore its method’s long-term efficacy, as recordings for each subject were collected during a single, 30-minute period.

Friedman et al. [24] employed a statistical approach for eye movement biometrics. A novel event classification algorithm, the modified Nyström and Holmqvist (MNH) algorithm [25], was used to classify several types of events. A set of over 1,000 features [26] was extracted from each recording. This approach was validated using a dataset of 298 subjects recorded twice each during a reading task. Using data separated by approximately 20 minutes, a best-case EER of 2.01% was reported. With data separated by approximately 11 months from a set of 68 subjects, EER increased to 10.16%.

Jäger et al. [28] utilized involuntary micro eye movements for biometric authentication and identification. Raw eye movement signals were initially transformed to isolate desired micro eye movements according to their characteristic velocities, with the resulting scaled values fed into a deep convolutional neural network (CNN) with two separate subnets. The approach was validated using two datasets (75 subjects during a reading task recorded at 1000 Hz [29], and a newly recorded dataset consisting of 10 users). This approach was later extended into DeepEyedentificationLive [4] to include liveness detection and was evaluated on a different dataset of 150 subjects, the JuDo1000 dataset [4], which is publicly available. But the EERs presented in the later study were based on only 1 genuine (enrolled) identity and 24 impostor identities, and the recordings were collected with a relatively short temporal separation.

Abdelwahab & Landwehr [12] introduced metric learning to the eye movement biometrics literature using deep distributional embeddings. Namely, sequences of six-dimensional vectors (binocular gaze and pupil data) at 30 Hz were fed to a deep neural network which produced distributional embeddings using a Wasserstein distance metric. The approach was validated on the publicly-available Dynamic Images and Eye Movements (DIEM) dataset [27], which contains eye movement data of 210 subjects viewing various video clips (sports, movie trailers, etc.). The recordings in the DIEM dataset were collected with only a small temporal separation.

Lohr et al. [13] also explored the use of metric learning for eye movement biometrics. Eye movement recordings were segmented into fixations, saccades, and PSOs using the MNH algorithm [25], and discrete feature vectors were extracted from each event. Three separate multilayer perceptrons (MLPs), one for each of the 3 event types, were trained on these feature vectors with triplet loss [7] to create meaningful embeddings. Distances were computed for each event type separately and then fused with a weighted sum. The approach was validated using a dataset of 269 subjects recorded twice each during a reading task. An average EER of 6.29% was reported for recordings separated by approximately 20 minutes. Like most prior studies, the permanence of eye movements was not explored.

The technique described herein expands upon the work of Lohr et al. [13] by feeding recordings directly into the model (removing the additional complexity of event classification), using the more sophisticated multi-similarity (MS) loss [10], training a single CNN rather than multiple event-specific MLPs, and assessing the performance of the model on a longitudinal dataset collected over a 37-month period. The present study also explores the authentication performance of additional tasks other than reading and of downsampled eye movement signals.

### 3 Methodology

#### 3.1 Dataset

We used the GazeBase [14] dataset available on Figshare [30]. This dataset consists of 322 college-aged subjects, each recorded monocularly (left eye only) at 1000 Hz with an EyeLink 1000 eye tracker. Nine rounds of recordings (R1–9) were captured over a period of 37 months, so this dataset enables us to evaluate how well a model generalizes long-term. Each subsequent round comprises a subset of subjects from the preceding round (with one exception, subject 76, who was not present in R3 but returned for R4 and R5), with only 14 of the initial 322 subjects present across all 9 rounds. Each round consists of 2 recording sessions separated by approximately 30 minutes, totaling 18 recording sessions. Recordings contain the horizontal and vertical components of the left eye’s gaze position in terms of degrees of the visual angle. In each recording session, every subject performed a series of 7 eye movement tasks: a horizontal saccade task (HSS), a video viewing task (VD1), a fixation task (FXS), a random saccade task (RAN), a reading task (TEX), a ball-popping task (BLG), and another video viewing task (VD2). A brief description of each task is given below, but more details can be found in [14].

For HSS, a white, bullseye target (approximately  $1^\circ$  in diameter) on a black background jumped between two fixed positions located at  $\pm 15^\circ$  of the visual angle, with each jump occurring at regular, one-second intervals. The target started at the center of the screen before making the first jump, and a total of 100 jumps were made. The task had a duration of 101 seconds.

For VD1, the first 60 seconds were shown of a trailer for the movie, “The Hobbit: The Desolation of Smaug.” No audio was played during the recording. During the second session of each round, only the first 57 seconds were shown due to variability in instrumentation settings. Since VD2 was similar to VD1, we only used VD1 in our experiments.

For FXS, a white, bullseye target (approximately  $1^\circ$  in diameter) on a black background was displayed at the center of the screen for a duration of 15 seconds.

For RAN, a white, bullseye target (approximately  $1^\circ$  in diameter) on a black background jumped between random positions restricted within a region from  $\pm 15^\circ$  horizontally and  $\pm 9^\circ$  vertically. The minimum amplitude between consecutive positions was  $2^\circ$ , and the positions were randomized for each recording. Like HSS, each jump occurred at regular, one-second intervals, and the target started at the center of the screen before making the first jump. A total of 100 jumps were made, resulting in a duration of 101 seconds.

For TEX, an excerpt from Lewis Carroll’s poem, “The Hunting of the Snark,” was displayed for 60 seconds with white font on a black background. A different excerpt was used for each recording session (i.e., 18 excerpts in all), and the same pair of excerpts was shown to all participants within a round.

For BLG, blue and red balls moving at a slow, fixed speed were displayed on the screen. Each ball was assigned a random trajectory at the beginning of the game and, upon reaching an edge of the display, bounced off the edge to prevent the ball from going off-screen. The goal of the game was to pop all the red balls by fixating on them. The blue balls could not be popped, but they were outlined in green when fixated on to provide visual feedback to the participant. This task had a variable duration dependent on how quickly each participant was able to pop all the red balls.

#### 3.2 Sampling rate degradation

The GazeBase dataset contains recordings of very high signal quality [31] recorded with an EyeLink 1000 eye tracker. Other eye trackers, such as Magic Leap One [32] or Vive Pro Eye [33], have lower signal quality (e.g., 60 Hz for the Magic Leap One or 120 Hz for the Vive Pro Eye). It is expected that in the future, eye tracking would become ubiquitous in virtual- and augmented-reality head-mounted displays due to the many benefits it could bring, including foveated rendering, continuous authentication, and increased immersion in video games. But since eye tracking signal quality varies between devices, in this study, it was important to consider how signal quality (specifically, sampling rate) impacts authentication performance. To this end, we downsampled the eye movement signals with an anti-aliasing filter. We targeted sampling rates of 500, 250, 125, 50, and 31.25 Hz. We chose 31.25 Hz instead of 30 Hz to simplify the downsampling process.

### 3.3 Training and testing splits

The subjects in the dataset were split in the following manner. First, we created a held-out test set using the 14 subjects that were present in all 9 rounds. The test set was only used at the very end of our experiments to get a final, unbiased measure of our models’ performance.

Next, we split the remaining subjects into 10 folds (which we will label F01–10) for cross-validation. We had three goals when balancing the folds, keeping in mind that some subjects have more recordings than others: (1) each fold should have a similar number of subjects, (2) each fold should have a similar number of recordings, and (3) the method to create the folds should be deterministic to facilitate reproducibility.

We accomplished these goals by using two priority queues (heaps)—one for the folds and the other for the subjects—and iteratively assigning subjects to folds. Each fold was weighted first by the number of subjects assigned to it and second by the total number of recordings present for those subjects, and the fold with the lowest weight was given the highest priority. Each subject was weighted by the total number of recordings present for that subject, and the subject with the highest weight was given the highest priority. In case of ties, an arbitrary-but-deterministic element was given higher priority. At each iteration, we extracted the highest priority element from both heaps and assigned the chosen subject to the chosen fold. The chosen fold was then placed back onto the heap with its updated priority. This process was repeated until the subject heap was empty. In the end, the largest fold had at most 1 more subject than the smallest fold, and the number of recordings present in each fold was as balanced as possible.

We ran three sets of experiments: (1) compare our metric learning model against a statistical baseline model, using data from TEX and tuning hyperparameters based on the average performance across the 10 folds; (2) use data from the other individual tasks to assess our model’s performance on types of eye movements other than reading; and (3) downsample the TEX data to assess our model’s performance on signals with lower sampling rates.

### 3.4 Signal pre-processing

We computed channel-wise sample-to-sample differences scaled by the sampling rate (i.e., instantaneous velocity) and used the resulting velocity signals rather than the raw positional signals. A NaN value was prepended to the velocity signal to preserve the original length of the recording.

All recordings in the training set were concatenated together to compute a channel-wise mean and standard deviation, which was used to z-score scale the signals in the training, validation, and test set. A separate z-score transformation was applied for each of the 10 models trained during 10-fold cross-validation, since the training sets differed between models. NaN values were ignored when determining the mean and standard deviation.

Before feeding data into the model, any NaN values were replaced with 0.

### 3.5 Multi-similarity loss

MS loss [10], like many other metric learning loss functions, is embedding-based (in contrast to classification-based losses like cross-entropy) [34] and pair-based. Minibatches are constructed from  $k$  samples each from  $n$  subjects so that both inter- and intra-class variations can be observed. Pairs of samples are constructed within each minibatch. A pair is *positive* if samples in the pair are from the same class or *negative* if they are from different classes. The goal is to bring positive pairs closer together in the embedding space and to push negative pairs farther apart. In other words, we want to construct a well-clustered embedding space. One challenge with pair-based losses is selecting the most informative pairs to accelerate learning. Using pairs that are too easy does not help the model learn, and using pairs that are too hard may lead to instability during training [35].

MS loss takes into account three different types of similarities: self-similarity, positive relative similarity, and negative relative similarity. This is a more sophisticated approach than most other losses that focus on either self-similarity (e.g., contrastive loss [36]) or relative similarity (e.g., triplet loss [7]) but not both. The most informative pairs are selected with an online pair mining technique and assigned similarity-based weights that decay exponentially as the pairs become less informative. A larger weight is given to positive pairs with low similarity and to negative pairs with high similarity. Together, these aspects help MS loss form a well-clustered embedding space and overcome the challenge of selecting informative pairs. MS loss is formulated as

$$L = \frac{1}{m} \sum_{i=1}^m \left( \frac{1}{\alpha} \log(1 + \sum_{k \in P_i} e^{-\alpha(S_{ik} - \lambda)}) + \frac{1}{\beta} \log(1 + \sum_{k \in N_i} e^{\beta(S_{ik} - \lambda)}) \right), \quad (1)$$

Table 2: The best set of hyperparameters found for TEX @ 1000 Hz after 60 iterations of random search.  
 \*: rounded to 3 significant figures (actual values used were not rounded).

Hyperparameter	Value
$w$	8000
$n$	8
$k$	4
learning rate*	$1.30 \times 10^{-4}$
weight decay*	$1.19 \times 10^{-4}$
gamma*	0.998
dilation	7
kernel size	7
global pooling	True
conv. filters	[64, 64, 64, 64]
linear layers	[128, 128]

where  $\alpha, \beta, \lambda$  are hyperparameters,  $m$  is the size of the minibatch,  $P_i$  and  $N_i$  are the sets of indices of the mined positive and negative pairs for each anchor sample  $\mathbf{x}_i$ , and  $S_{ik}$  is the cosine similarity between the pair of samples  $\{\mathbf{x}_i, \mathbf{x}_k\}$ . For more technical details and descriptive figures, please refer to the MS loss paper [10].

Although the latest metric learning loss functions (such as MS loss) may not improve upon earlier loss functions as much as the literature would suggest [34], many (including MS loss) do appear to lead to marginal improvements over cross-entropy or triplet loss after controlling for several factors including network architecture, batch size, and optimizer.

### 3.6 Hyperparameter tuning

We performed 60 iterations of random search [37] on a large hyperparameter space. By running 60 iterations of random search, there is a 95% chance of finding a combination of hyperparameters that lies within the top 5% of all hyperparameter combinations. But due to our large search space, it may be the case that only the top 1% (or 0.1%, etc.) of hyperparameter combinations produce reasonable results; so, more than 60 iterations may be necessary to find a good set of hyperparameters.

At each search iteration, a random set of hyperparameters within the search space was chosen. A total of 10 models were trained with the selected hyperparameters, with a different fold being used as the validation set for each model (and the remaining folds being used for training). Performance metrics were computed on the validation set after every 1,000 training steps. Rather than training for a fixed number of steps, early stopping was used with a patience of 10 performance evaluations (10,000 steps) based on EER of the validation set. The best performing model for each validation fold was kept at each search iteration. For more details about training, see Section 3.8.

We evaluated 60 different sets of hyperparameters in this manner (a total of 600 models). The set of hyperparameters that minimized  $mean(EER) + 1.96 \times sd(EER)$  across the 10 models was used during our final analyses. The hyperparameter search space is provided in the supplementary material, and the set of hyperparameters that we used for TEX @ 1000 Hz is shown in Table 2.

The above is true for TEX @ 1000 Hz. For all other tasks and sampling rates, in the interest of time, we opted to train only one model per search iteration (training on F02–F10 and validating on F01) rather than 10 models.

Sometimes, a combination of hyperparameters was invalid (e.g., too many dilated convolutional layers with too small a window size) or required more GPU memory than was available. In such cases, we skipped that search iteration. Additionally, for TEX @ 31.25 Hz, the “best” set of hyperparameters was a fluke (most genuine pairs had similarity 1.000000 and most impostor pairs had similarity 0.999999, so there was not a real, clear separation between genuine and impostor pairs, but EER was very low). So, for TEX @ 31.25 Hz only, we used the second-best set of hyperparameters.

### 3.7 Network architecture

We used a neural network with an architecture determined by our random search procedure described in the previous section. In general, the network started with some number of (dilated) convolutional layers, optionally followed by global max pooling, followed by some number of linear/fully-connected layers. Each convolutional layer used the ReLU activation function followed by batch normalization (though, there is some debate whether batch normalization should

appear before or after the activation function). All fully-connected layers except the last used the ReLU activation function. The output of the last fully-connected layer was L2-normalized to constrain embeddings to the surface of a hypersphere.

As an example, the specific architecture found for TEX @ 1000 Hz is described below. The network started with four 1D convolutional layers, each with 64 filters, a kernel size of 7, and a dilation of 7. The purpose of using dilated convolutions was to expand the perceptive view of each filter without increasing the number of learnable parameters. Each convolutional layer used the ReLU activation function followed by batch normalization. Global max pooling was applied to the output of the last convolutional layer, resulting in one value per filter. The result was then flattened into a one-dimensional array and fed into 2 fully-connected layers to produce the final embedding of the input. Both fully-connected layers had size 128. The first one used the ReLU activation function, while the second (acting as the embedding layer) did not use an activation function. The output of the network was L2-normalized to constrain embeddings to the surface of a 128-dimensional hypersphere.

### 3.8 Training

We trained 10 different models, each one using a different held-out fold as the validation set and the remaining 9 folds as the training set. The data were z-score scaled using the mean and standard deviation of the model’s training set.

We used the AdamW [38] optimizer with learning rate and weight decay determined via random search (for TEX @ 1000 Hz, learning rate was  $1.30 \times 10^{-4}$  and weight decay was  $1.19 \times 10^{-4}$ ). All other optimizer hyperparameters were left at their default values. We used multi-similarity (MS) loss [10] with an online miner as implemented in the PyTorch Metric Learning (PML) library [39]. The hyperparameters for MS loss were left to their PML-default values ( $\alpha = 2$ ,  $\beta = 50$ ,  $\lambda = 0.5$ ,  $\epsilon = 0.1$ ).

At each training step, we sampled a minibatch comprising  $k$  subsequences each from  $n$  subjects, with  $k, n$  determined during the random search procedure (for TEX @ 1000 Hz,  $k = 4$  and  $n = 8$ ). Each subsequence had length  $w$  determined during the random search procedure (for TEX @ 1000 Hz,  $w = 8000$  ms). First, the  $n$  subjects were chosen. Then, for each subject, the  $k$  subsequences were independently sampled from all recordings of that subject. Rather than sampling from only the non-overlapping subsequences, the subsequences used during training were chosen from arbitrary positions in each recording. This forces the network to learn similarities (and differences) between arbitrary subsequences of eye movements during the task and across recording sessions, hopefully improving its ability to generalize to new subjects.

After every 1,000 training steps, the model’s performance was evaluated on the validation set. Early stopping with a patience of 10 performance evaluations (10,000 steps) based on EER of the validation set was used to determine when to stop training. The learning rate was decayed by a constant factor  $\gamma$  (determined during the random search procedure) after every 1,000 training steps (for TEX @ 1000 Hz,  $\gamma = 0.998$ ).

### 3.9 Evaluation

To get the final embedding of each recording, we split the recording into all non-overlapping subsequences of length  $w$ , fed each subsequence into the model to get an embedding for that subsequence, and then took the mean of all subsequences to get a centroid embedding. The centroid embedding was then L2-normalized, just as the individual subsequence embeddings were.

There are two main scenarios for biometrics: authentication and identification. In the authentication scenario, a user attempts to access a system by claiming to be a specific enrolled user and presenting their biometric sample (e.g., a fingerprint), and a decision is made based on the sample’s similarity to the biometric template of that specific enrolled user. In the identification scenario, a user attempts to access a system by claiming to be *any* enrolled user and presenting their biometric sample, which is then compared against the biometric template of *every* enrolled user to see if there is any match. As more users are enrolled, it becomes increasingly difficult to detect impostors in the identification scenario, as the impostor’s presented biometric sample need only be similar to any one enrolled user’s biometric template. This phenomenon has been formally studied using synthetic and real datasets [40]. Therefore, we consider only the authentication scenario, for which performance is expected to remain relatively consistent regardless of the number of enrolled users [40].

An important consideration for any biometric modality is how it compares to existing security methods. For example, the 4-digit pin is one of the most common security methods for smartphones and is often used as a backup authentication method if biometrics fail. If a biometric modality is less secure than a 4-digit pin, it would have little practical benefit on its own. There are  $10^4$  possible ways to construct a 4-digit pin with the numbers 0–9, so assuming each pin is equally likely to be chosen, there is a  $10^{-4}$  chance that an impostor would correctly guess a specific user’s pin. Therefore, we

provide measures of false rejection rate (FRR) when false acceptance rate (FAR) is fixed at  $10^{-4}$ , abbreviated FRR @ FAR  $10^{-4}$ . According to the FIDO Biometrics Requirements [41], a biometric system should achieve a FRR @ FAR  $10^{-4}$  of no more than 5%.

We created genuine and impostor pairs in a manner inspired by the fingerprint verification pipeline from Cappelli et al. [42]. Using that pipeline, genuine pairs are formed by comparing each fingerprint image against each other image from the same finger (discarding redundant pairs), and impostor pairs are formed by comparing the first image of each finger against the first image of all other fingers (discarding redundant pairs). In terms of the present study, each “finger” is a subject, and each “fingerprint image” corresponds to an eye movement recording. If we used all available recordings in our test set (14 subjects each recorded a total of 18 times), we would have had  $\binom{18}{2} \times 14 = 2,142$  genuine pairs and  $\binom{14}{2} = 182$  impostor pairs by following the pipeline from [42]. This is significantly fewer than the 10,000 impostor pairs that were needed to estimate FRR @ FAR  $10^{-4}$ . While we could have performed bootstrapping to artificially inflate the number of impostor pairs, we instead chose to adjust the technique for creating impostor pairs.

Genuine pairs were created by comparing every recording from each subject to every other recording from the same subject and discarding any redundant pairs. This is identical to the approach by [42]. In general, this results in

$$\sum_{i=1}^N \binom{|S_i|}{2} = \frac{1}{2} \sum_{i=1}^N |S_i| \cdot (|S_i| - 1) \quad (2)$$

genuine pairs, where  $N$  is the number of unique subjects and  $|S_i|$  is the number of recordings available for subject  $i$ . For the test set, which contains 14 subjects each with 18 recordings, there are 2,142 genuine pairs.

Impostor pairs were created by comparing the first session recording of each round of each subject against the second session recording of each round of every other subject. In general, assuming there are 2 recording sessions per round (as is the case for GazeBase), this results in

$$\frac{1}{4} \sum_{i=1}^N \sum_{\substack{j=1 \\ j \neq i}}^N |S_i| \cdot |S_j| \quad (3)$$

impostor pairs, where  $N$  is the number of unique subjects and  $|S_i|$  is the number of recordings available for subject  $i$ . For the test set, which contains 14 subjects each with 18 recordings across 9 rounds, there are 14,742 impostor pairs.

For each validation set, approximately 10% of the pairs were genuine and the other 90% of the pairs were impostors. For the test set, a little under 13% of the pairs were genuine and a little over 87% of the pairs were impostors.

We used these genuine and impostor pairs to build a receiver operating characteristic (ROC) curve for each model to determine the tradeoff between FRR and FAR. FRR is the rate at which a genuine authentication attempt fails (i.e., the similarity of a genuine pair is below a threshold), while FAR is the rate at which an impostor authentication attempt succeeds (i.e., the similarity of an impostor pair is above a threshold). The ROC curve reveals how FRR and FAR are affected as the similarity threshold changes. From the ROC curve, we determined the equal error rate (EER)—the point where FRR equals FAR—as well as FRR at a fixed FAR (abbreviated FRR @ FAR).

Since cosine similarity was used for MS loss, we also used cosine similarity (derived from Euclidean distance) for the match scores in the ROC analyses. Consider a pair of  $\ell^2$ -normalized embeddings  $\mathbf{a}, \mathbf{b} \in \mathbb{R}^d$  where  $\|\mathbf{a}\|_2 = \|\mathbf{b}\|_2 = 1$ . The distance  $D$  between  $\mathbf{a}$  and  $\mathbf{b}$  and the corresponding similarity  $S$  are given in Equation 4 below.

$$D = \|\mathbf{a} - \mathbf{b}\|_2 = \sqrt{\sum_{i=1}^d (\mathbf{a}_i - \mathbf{b}_i)^2} \quad (4)$$

$$S = 1 - \frac{D^2}{2}$$

$S$  is identical to cosine similarity, but we opted to use Euclidean distance as a proxy since we found greater support for the latter in PyTorch (namely, the functions `pdist` and `cdist`). Since our ROC analyses encompassed both short- and long-term similarities (with temporal separations ranging from 30 minutes to 37 months), the results provide an overall expected level of performance of our models over time. We would expect short-term similarities to be higher than long-term similarities for genuine pairs.

### 3.10 Statistical baseline

We compare our metric learning approach against a statistical baseline based on [24] that we will refer to as STAR. First, each recording was classified into fixations, saccades, post-saccadic oscillations (PSOs), and noise using the modified



Nyström and Holmqvist (MNH) classification algorithm [25]. Next, for each recording, a set of over 1,000 features [26] was extracted from the classified events. The same 10 folds and test set were used for STAR as were used for our metric learning approach. The features in the training set were combined into a matrix, where each row was a recording and each column was a feature. The same was done for the validation and test set.

The large number of features was reduced in the following manner (when we refer to a feature here, we are referring to the entire column in the matrix, i.e., the distribution of the feature across recordings). First, a feature was removed if any value was non-finite (infinite or NaN), or if all values were the same (e.g., all 0). Next, the Box-Cox transformation was applied to each feature to attempt to make its distribution across recordings more Gaussian. Since Box-Cox requires strictly positive values, a feature with non-positive values (including 0) were shifted by their minimum value to make them strictly positive. Features that were already strictly positive were not shifted.

Normality was tested by comparing the skewness and kurtosis of the feature distribution against the range of the skewness and kurtosis values seen across 10,000 randomly generated normal distributions with the same sample size. Features that were not sufficiently normal (i.e., their skewness and/or kurtosis did not lie within the appropriate range) were removed. The remaining features were then z-score transformed.

Then, the reliability of each feature was measured using the intraclass correlation coefficient (ICC). Since there is a lot of “missing” data (only a small portion of subjects were present in all rounds), reliability was measured within only the first round for a stronger analysis. Though it is possible to work around missing data, there is a substantial amount of missing data in this case, and it is systematic (e.g., if a recording is not present in the second round, then it will also not be present in any later rounds), so this potentially complicates the use of a reliability measure across all rounds. Any features with a negative reliability were removed.

Next, redundant features were removed. There were two types of redundancy: “structural” redundancy (i.e., both the mean and median or both the standard deviation (SD) and interquartile range (IQR) of the same underlying feature) and “effective” redundancy (i.e., features that were highly correlated). Structural redundancies were removed by finding instances where both the mean and median (or the SD and IQR) of the same underlying feature were present and removing the one with lower reliability. Effective redundancies were then removed by finding the two most highly correlated features, removing the one with lower reliability, and repeating until all features had correlation below 0.9.

Lastly, the remaining feature matrix was checked for positive definiteness. If it was not, the two most highly correlated features were selected, the one with lower reliability was removed, and this process was repeated until the feature matrix was positive definite. Though, in the present study, the feature matrices were always already positive definite.

Next began the optimization phase. The features in the validation set were reduced to the same set of features that remained in the training set. Since a feature may be strictly positive in the training set but not in the validation set, a different offset was applied before transforming with Box-Cox (using the power parameter fit on the training set) to ensure the features in the validation set were strictly positive. We started with the most reliable feature and iteratively added the next-most-reliable feature one at a time. Principal component analysis (PCA) was performed on the selected features in the training set, and the same coefficients were then applied to the same features in the validation set. We started with the component that explained the most amount of variance and iteratively added the next-most-explanatory component one at a time. The combination of features and principal components that resulted in the lowest EER on the validation set was chosen to use on the held-out test set. This entire process was repeated a total of 10 times, with a different fold being used as the validation set each time.

To evaluate the model on the test set, the features in the test set were reduced to the optimal set of features found for the validation set. The features in the test set were offset to ensure they were strictly positive before transforming with Box-Cox (using the power parameter fit on the training set). The PCA coefficients from the training set were applied to the test set, and the optimal number of principal components (determined during the optimization phase) was used. EER was computed on the test set using the same genuine and impostor pairs described in Section 3.9, except cosine similarity was computed directly.

### 3.11 Hardware & software

Training of the metric learning models was done on two Lambda Labs workstations. One workstation was equipped with dual NVIDIA GeForce RTX 2080 Ti GPUs (11 GB VRAM), an Intel i9-10920X CPU @ 3.50 GHz (12 cores), and 128 GB RAM. The other workstation was equipped with dual NVIDIA GeForce RTX 3080 GPUs (10 GB VRAM), an Intel i9-10900X CPU @ 3.70 GHz (20 cores), and 64 GB RAM. Both workstations ran Ubuntu 20.04 and used Python 3.6 and PML [39] version 0.9.92. The first workstation used PyTorch 1.6, but the other workstation used PyTorch 1.8 due to incompatibilities between PyTorch 1.6 and the RTX 3080.

Table 3: Performance measures computed on the held-out test set using TEX @ 1000 Hz. Values are given as mean  $\pm$  standard deviation, aggregated across 10 models trained via 10-fold cross-validation.

Model	EER	FRR @ FAR			
		$10^{-1}$	$10^{-2}$	$10^{-3}$	$10^{-4}$
Metric Learning	$0.0322 \pm 0.0054$	$0.0080 \pm 0.0065$	$0.0779 \pm 0.0170$	$0.2336 \pm 0.0459$	$0.3638 \pm 0.0727$
STAR	$0.1436 \pm 0.0102$	$0.1855 \pm 0.0191$	$0.4763 \pm 0.0393$	$0.7047 \pm 0.0570$	$0.8569 \pm 0.0667$

For TEX @ 1000 Hz, the 60 iterations of random search on all 10 folds took approximately 2 weeks to complete on a single GPU, and each model with the final hyperparameter configuration took an average of 23 minutes to train. For all other tasks and sampling rates, where we ran the 60 iterations of random search with only F01 as the validation set, all hyperparameter searches finished within a couple days spread across all GPUs.

STAR was run on a computer running Windows 10, equipped with an Intel i7-6700K CPU @ 4.00 GHz (4 cores) and 16 GB RAM. The code was written in MATLAB 2020a and ran serially on the CPU. Each model took approximately 10 minutes to train, with most of the time being spent in the optimization stage.

## 4 Results

The average performance measures of our approach and the STAR baseline on the held-out test set are given in Table 3. Comparisons between different tasks are provided in Table 4 and between different sampling rates in Table 5. Performance is assessed qualitatively by plotting the similarity distributions for genuine and impostor pairs in Fig. 1 and by plotting the ROC curves in Fig. 2. We noticed that our metric learning models tended to perform better with longer input sequences and with global max pooling applied before the first fully-connected layer. All 10 STAR models preferred to include all available features as input to PCA, but the optimal number of principal components varied between models.

Keep in mind that the hyperparameters for TEX @ 1000 Hz were tuned based on the average validation performance across 10 models, while the hyperparameters for all other tasks and sampling rates were tuned based on the validation performance of a single model (trained on F02–F10 and validated on F01).

We also wanted to see how well the models would do with less data available at enrollment and authentication time. So, we evaluated each model (except STAR) using only the first window of each recording (see Table 6). This comparison also accounts for the large differences in task duration.

For a statistical analysis of the results, we refer to the effect of each experiment as Condition and to the effect of each of the 10 EER estimates per experiment as Estimate. That is, each Condition had 10 Estimates, and there were a total of 12 Conditions (TEX @ 1000 Hz, 5 additional tasks, 5 additional sampling rates, and the STAR method). We performed a mixed model ANOVA in SAS with Estimate as a random effect and Condition as a fixed effect. We used an unstructured covariance structure. The ANOVA was followed by lsmeans estimates of all Condition by Condition contrasts, with multiple comparisons controlled for by Scheffé’s method.

Regarding the results presented in Table 3, we found that EER was significantly lower for our metric learning approach than the STAR approach ( $t(103.4) = -27.04$ ,  $p < .0001$ ).

Regarding the results from different tasks presented in Table 4, we found that EER was significantly lower for HSS than VD1 ( $t(103.4) = -22.47$ ,  $p < .0001$ ) and FXS ( $t(103.4) = -34.20$ ,  $p < .0001$ ). The EERs from the other tasks (RAN, TEX, and BLG) were not significantly different from HSS.

Regarding the results from different sampling rates presented in Table 5, we found that EER was significantly lower for 1000 Hz than all other sampling rates (all  $p < .001$ ). 50 Hz had significantly lower EER than everything but 1000 Hz (all  $p < .002$ ). 125 Hz had significantly lower EER than 500 Hz ( $t(103.4) = 6.02$ ,  $p = .0007$ ) and 250 Hz ( $t(103.4) = 4.83$ ,  $p = .0247$ ).

We did not perform statistical tests for the first-window-only results shown in Table 6.

Table 4: Performance measures computed on the held-out test set for each task at the native 1000 Hz sampling rate. Rows are ordered following the task order during the recordings. Values are given as mean  $\pm$  standard deviation, aggregated across 10 models trained via 10-fold cross-validation. Bold values indicate the best in each column.  
\*: mean and standard deviation of task duration across all recordings in the dataset.

Task	Duration* (s)	EER	FRR @ FAR			
			$10^{-1}$	$10^{-2}$	$10^{-3}$	$10^{-4}$
HSS	101.319 $\pm$ 0.080	<b>0.0304 <math>\pm</math> 0.0061</b>	<b>0.0049 <math>\pm</math> 0.0035</b>	0.0878 $\pm$ 0.0269	<b>0.2260 <math>\pm</math> 0.0572</b>	0.3682 $\pm$ 0.0975
VD1	58.584 $\pm$ 1.500	0.1231 $\pm$ 0.0151	0.1544 $\pm$ 0.0369	0.5256 $\pm$ 0.0648	0.7877 $\pm$ 0.0414	0.8977 $\pm$ 0.0285
FXS	15.079 $\pm$ 0.005	0.1714 $\pm$ 0.0081	0.2829 $\pm$ 0.0227	0.7213 $\pm$ 0.0511	0.9132 $\pm$ 0.0334	0.9711 $\pm$ 0.0174
RAN	101.102 $\pm$ 0.037	0.0402 $\pm$ 0.0060	0.0138 $\pm$ 0.0064	0.1210 $\pm$ 0.0196	0.2937 $\pm$ 0.0545	0.4647 $\pm$ 0.0710
TEX	60.242 $\pm$ 0.046	0.0322 $\pm$ 0.0054	0.0080 $\pm$ 0.0065	<b>0.0779 <math>\pm</math> 0.0170</b>	0.2336 $\pm$ 0.0459	<b>0.3638 <math>\pm</math> 0.0727</b>
BLG	37.276 $\pm$ 20.042	0.0424 $\pm$ 0.0039	0.0105 $\pm$ 0.0042	0.1796 $\pm$ 0.0511	0.4555 $\pm$ 0.0691	0.7583 $\pm$ 0.1035

Table 5: Performance measures computed on the held-out test set for TEX at various degraded sampling rates. Rows are ordered by decreasing sampling rate. Values are given as mean  $\pm$  standard deviation, aggregated across 10 models trained via 10-fold cross-validation. Bold values indicate the best in each column.

Sampling rate (Hz)	EER	FRR @ FAR			
		$10^{-1}$	$10^{-2}$	$10^{-3}$	$10^{-4}$
1000	<b>0.0322 <math>\pm</math> 0.0054</b>	<b>0.0080 <math>\pm</math> 0.0065</b>	<b>0.0779 <math>\pm</math> 0.0170</b>	<b>0.2336 <math>\pm</math> 0.0459</b>	<b>0.3638 <math>\pm</math> 0.0727</b>
500	0.1051 $\pm$ 0.0086	0.1058 $\pm$ 0.0118	0.2033 $\pm$ 0.0276	0.9987 $\pm$ 0.0002	0.9996 $\pm$ 0.0003
250	0.1003 $\pm$ 0.0049	0.1001 $\pm$ 0.0078	0.2094 $\pm$ 0.0257	0.9984 $\pm$ 0.0004	0.9995 $\pm$ 0.0003
125	0.0803 $\pm$ 0.0054	0.0666 $\pm$ 0.0086	0.2541 $\pm$ 0.0558	0.9957 $\pm$ 0.0005	0.9988 $\pm$ 0.0006
50	0.0568 $\pm$ 0.0061	0.0245 $\pm$ 0.0077	0.2780 $\pm$ 0.0234	0.8314 $\pm$ 0.0377	0.9614 $\pm$ 0.0136
31.25	0.3689 $\pm$ 0.0186	0.7243 $\pm$ 0.0405	0.9581 $\pm$ 0.0218	0.9936 $\pm$ 0.0049	0.9980 $\pm$ 0.0017

Table 6: Performance measures computed on the held-out test set for each task and at various degraded sampling rates when using only the first window of data. Values are given as mean  $\pm$  standard deviation, aggregated across 10 models trained via 10-fold cross-validation. Bold values indicate the best in each column.

Task	Sampling rate (Hz)	Window size (s)	EER	FRR @ FAR			
				$10^{-1}$	$10^{-2}$	$10^{-3}$	$10^{-4}$
HSS	1000	8	<b>0.0684 <math>\pm</math> 0.0068</b>	<b>0.0470 <math>\pm</math> 0.0105</b>	<b>0.2416 <math>\pm</math> 0.0305</b>	<b>0.5042 <math>\pm</math> 0.0432</b>	<b>0.6784 <math>\pm</math> 0.0620</b>
VD1	1000	10	0.2109 $\pm$ 0.0191	0.3944 $\pm$ 0.0454	0.8014 $\pm$ 0.0286	0.9498 $\pm$ 0.0111	0.9835 $\pm$ 0.0089
FXS	1000	7	0.1843 $\pm$ 0.0072	0.3330 $\pm$ 0.0261	0.7874 $\pm$ 0.0442	0.9449 $\pm$ 0.0220	0.9848 $\pm$ 0.0086
RAN	1000	9	0.0997 $\pm$ 0.0114	0.1003 $\pm$ 0.0227	0.4043 $\pm$ 0.0357	0.6851 $\pm$ 0.0455	0.8427 $\pm$ 0.0329
TEX	1000	8	0.0880 $\pm$ 0.0063	0.0786 $\pm$ 0.0111	0.3603 $\pm$ 0.0399	0.6558 $\pm$ 0.0580	0.8260 $\pm$ 0.0678
BLG	1000	6	0.0948 $\pm$ 0.0077	0.0898 $\pm$ 0.0159	0.4194 $\pm$ 0.0268	0.7130 $\pm$ 0.0329	0.8619 $\pm$ 0.0314
TEX	500	8	0.1446 $\pm$ 0.0140	0.1788 $\pm$ 0.0270	0.4818 $\pm$ 0.0485	0.8805 $\pm$ 0.0417	0.9986 $\pm$ 0.0027
TEX	250	6	0.1577 $\pm$ 0.0101	0.2222 $\pm$ 0.0218	0.5706 $\pm$ 0.0377	0.8159 $\pm$ 0.0412	0.9296 $\pm$ 0.0377
TEX	125	10	0.1020 $\pm$ 0.0094	0.1035 $\pm$ 0.0153	0.3051 $\pm$ 0.0337	0.5522 $\pm$ 0.0640	0.7116 $\pm$ 0.0828
TEX	50	8	0.1497 $\pm$ 0.0046	0.2115 $\pm$ 0.0106	0.5853 $\pm$ 0.0154	0.8244 $\pm$ 0.0181	0.9205 $\pm$ 0.0258
TEX	31.25	4	0.4358 $\pm$ 0.0141	0.8234 $\pm$ 0.0108	0.9780 $\pm$ 0.0072	0.9971 $\pm$ 0.0017	0.9992 $\pm$ 0.0008

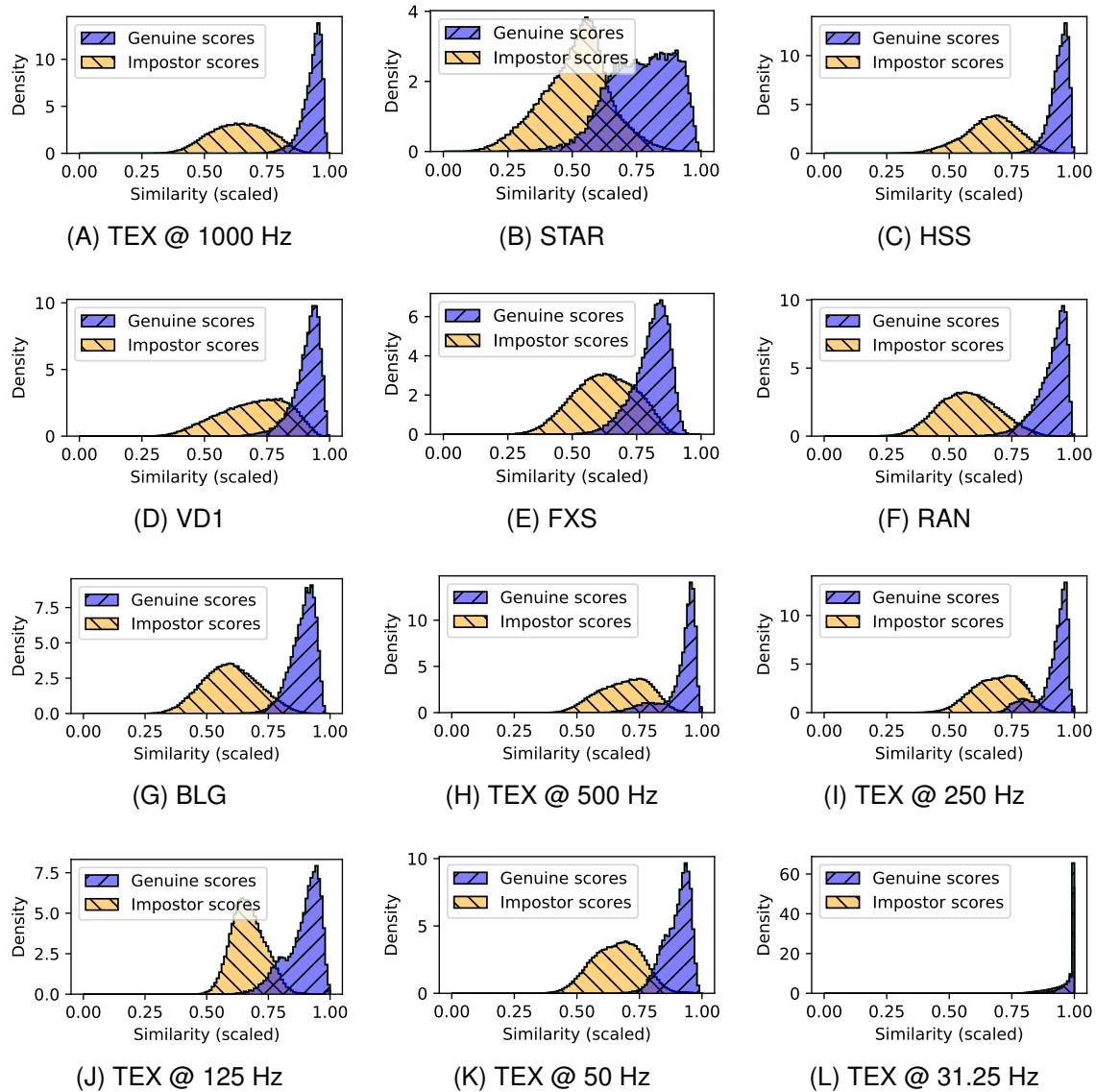


Figure 1: Plots of the similarity distributions for genuine and impostor pairs to provide a qualitative assessment of model performance. Each plot contains the similarities on the held-out test set computed separately for each of the 10 models trained with 10-fold cross-validation. Since similarity computed through cosine similarity is bounded from -1 to 1, we scaled the similarities to lie between 0 and 1 before plotting. A bin width of 0.01 was used, and the area under each curve sums to 1.

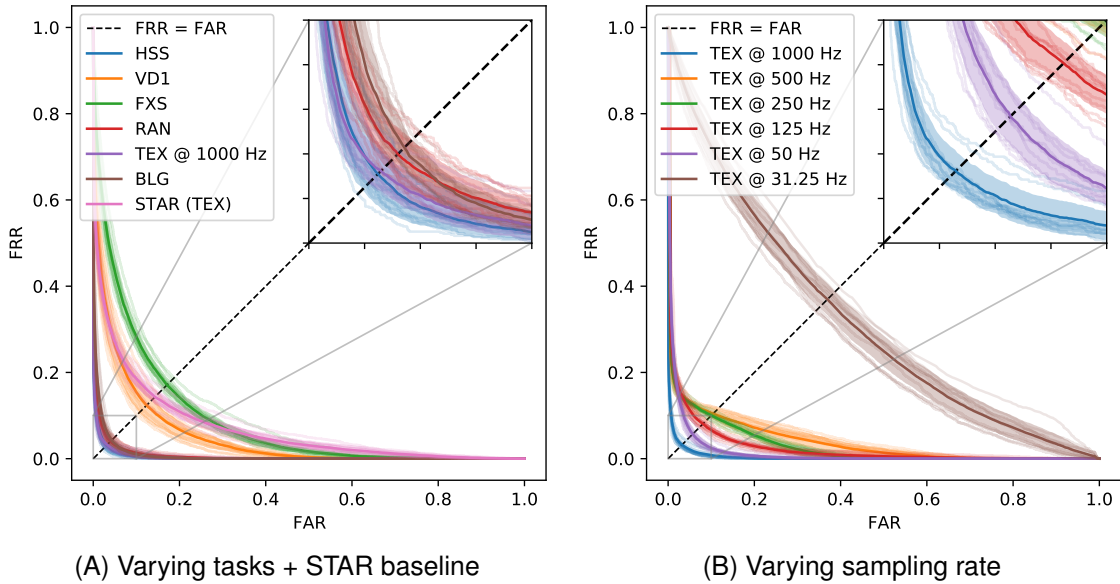


Figure 2: ROC curves to provide a qualitative assessment of model performance. The horizontal axis is false acceptance rate (FAR). The vertical axis is false rejection rate (FRR). A separate ROC curve is plotted for each of the 10 models trained with 10-fold cross-validation, and the mean ROC curve of these 10 curves is drawn with a thicker line. Each mean curve is surrounded by a shaded region indicating the standard deviation of the 10 curves. The point where the dashed line intersects each ROC curve indicates the EER for that curve. A zoom inset bounded from 0 to 0.1 on both axes is included at the top-right corner to help distinguish different curves.

## 5 Discussion

### 5.1 Comparison to state-of-the-art

We chose not to compare against the current state-of-the-art model, DeepEyedentificationLive [4], for a few reasons. First and foremost, there would be many confounding factors influencing any performance differences we may have found between our presented approach and DeepEyedentificationLive (this is often overlooked in studies comparing different models [34]). Aspects including but not limited to network architecture, input window length, training duration, optimizer, minibatch size, genuine and impostor pair formation, and dataset would all need to be controlled for in order for the comparison to be meaningful. Essentially, we would need to recreate their study, only replacing their classification-based loss with MS loss. While this would be possible, that leads to the second reason we did not include a comparison against the current state-of-the-art: we had difficulty recreating their methodology. Since no code is provided for DeepEyedentificationLive, we would have needed to start from scratch, which would take a non-trivial amount of time. Third, we found it problematic that their EER estimates were based on only 1 genuine (enrolled) identity and 24 impostor identities. Overall, we decided not to go forward with this comparison. But given code for their approach, it should be easy to incorporate MS loss and see how it affects the model’s performance.

### 5.2 Authentication accuracy vs sampling rate

It is interesting that there is not a monotonic increase in EER as the sampling rate is reduced (see Table 5). For example, TEX @ 50 Hz has a lower EER (5.7%) than at 125 Hz (8.0%), 250 Hz (10.0%), and 500 Hz (10.5%). While it may be the case that the filtering applied during downsampling was somehow beneficial for biometrics, we believe that the observed variability in EER is primarily due to the random aspect of our hyperparameter tuning approach and that highly impactful hyperparameters—including the number of layers in the network and the window size—were included in the search space.

We do see, though, that FRR @ FAR is heavily impacted by the reduction in sampling rate, with the exception of TEX @ 125 Hz when using only the first window of data (see Table 6). This outlier is likely due in large part to using a window of 10,000 ms for the models on 125 Hz data but only 8,000 ms for the models on 1000 Hz data.

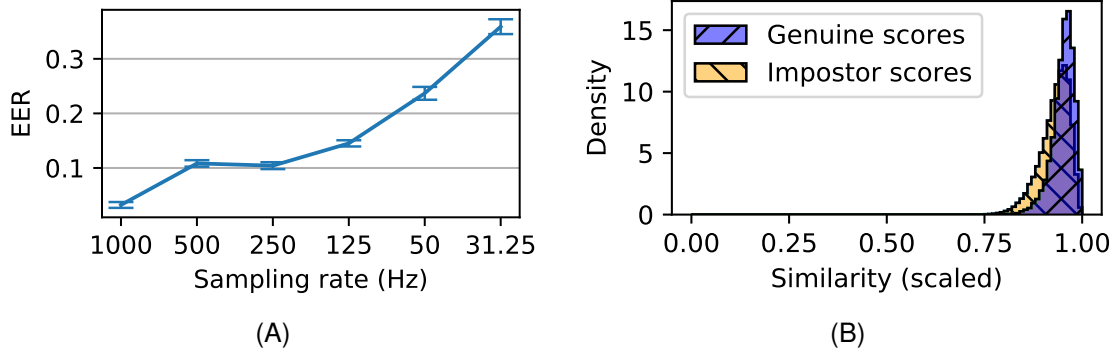


Figure 3: Authentication performance at degraded sampling rates when using the set of hyperparameters tuned on TEX @ 1000 Hz. (A) Change in EER for the TEX task as sampling rate is degraded. The plotted values are the mean EER across 10 models trained for each sampling rate, and error bars are  $\pm 1$  standard deviation. Note that there is a mostly monotonic increase in EER as would be expected. (B) A plot of the similarity distributions for genuine and impostor pairs for TEX @ 31.25 Hz. Note that the distributions are not as concentrated around 1.00 similarity as they are in Fig. 1L. See the caption of Fig. 1 for more details.

To account for variability due to random search, we re-trained the models for each degraded sampling rate using the same hyperparameters as TEX @ 1000 Hz. The only change made was to the window size, which was adjusted according to the sampling rate to keep the duration in milliseconds constant. Indeed, when the hyperparameters were kept constant, we saw a mostly monotonic increase in EER as the sampling rate was reduced (see Fig. 3A). The only exception was that TEX @ 250 Hz had a slightly lower EER than TEX @ 500 Hz, but the difference was within  $\pm 1$  standard deviation. Although these hyperparameters included a dilation of 7 which we expect would not be ideal for lower sampling rates, this comparison does show that the variability in performance across sampling rates seen in Table 5 is largely due to the hyperparameters used rather than some intrinsic benefit of downsampling the signals.

There is a steep drop in performance going from 50 Hz (5.7% EER) to 31.25 Hz (36.9% EER) (see Table 5). Looking at the similarity distributions in Figure 1L, it is clear that the models struggle to distinguish sequences at 31.25 Hz. We believe this is largely due to suboptimal hyperparameters being found for TEX @ 31.25 Hz. Many hyperparameter configurations were invalid for the 31.25 Hz data, and since we skipped search iterations with invalid configurations, there were not 60 valid search iterations performed for TEX @ 31.25 Hz. For example, a window size of 4,000 ms was used at 31.25 Hz, but given that the other TEX models all used at least 6,000-ms windows, it is likely that a larger window size would also lead to better performance at 31.25 Hz. When using the same hyperparameters as TEX @ 1000 Hz, we get the similarity distributions shown in Fig. 3B. With these hyperparameters, the model is able to find differences between input signals more easily (exhibited by the fact that the distributions are not as concentrated around 1.00 similarity). Though it is still difficult to distinguish the genuine and impostor distributions, this is likely caused in part by the use of a dilation of 7 for the convolutional layers.

### 5.3 Authentication accuracy vs task

Another interesting result is that HSS performed the best of all the tasks (see Table 4), especially when using only the first available window of data (see Table 6). We expected TEX to perform the best, since many studies in the past have shown the efficacy of eye movements during reading as a biometric [43, 24, 28, 13], and we also expected at least RAN to outperform HSS since RAN is less predictable. The difference in performance is not significant between HSS (3.0% EER) and TEX (3.2% EER) when using all windows (see Table 4), though HSS utilizes 101 seconds of data compared to 60 seconds for TEX. When using only the first window of data at evaluation time (see Table 6), the difference between HSS (6.8% EER) and TEX (8.8% EER) is substantial, which is surprising. Therefore, perhaps it is not necessary for participants to be under a high cognitive load in order to extract biometric information from their eye movement signals, and something as mundane as repeatedly looking left and right may be sufficient for authentication purposes.

While many prior studies have also used jumping dot tasks (e.g., [44, 4]), they would be considered more similar to RAN than HSS. HSS differs from most prior jumping dot tasks in that the movements are predictable. There is a 1 second delay between jumps, and the jumps alternate between the same two positions.

## 5.4 Comparison to STAR

Looking at Table 3, our metric learning model resulted in a statistically significant reduction of EER compared to the STAR baseline. Regarding the discrepancy between our results with STAR and the original results from [24] (where an EER of 10% was achieved on data separated by approximately 1 year), there are many contributing factors.

First, our EER estimates are based on different data than the original study. We used data from 14 subjects across all 9 rounds, did not remove signal after the end of reading, and did not exclude any subjects from the analysis regardless of data quality. In contrast, the original paper used either round 1 only (SBA-ST) or used one session each from round 1 and round 5 (SBA-LT), removed signal after the end of reading, and screened subjects with “low recording quality” or who had “excessively noisy recordings.”

Second, we made several changes to the original approach: we simplified the normality transformations by always using Box-Cox instead of trying several different standard transformation functions; we did not winsorize the distributions to try to improve normality; we tested normality by checking skewness and kurtosis instead of using the chi-square test; we measured reliability on a set of data disjoint from our test set; and we iteratively added the most reliable features until achieving optimal performance instead of using reliability intervals.

Third, we did not have access to several oculomotor plant characteristic (OPC) features that were present in the original study, some of which were found to be highly reliable in the original study.

## 5.5 Limitations

First, it is important to keep in mind that our EER estimates are based on only 14 subjects. Even though we were able to construct a reasonable number of genuine and impostor pairs for our ROC analyses, there is probably a decent amount of correlation between similarity measures. As a result, we cannot say with high confidence that our model would perform at a similar level on a different pool of subjects, because the size of our test set might not offer adequate support for such a claim.

Second, there is an implicit assumption when averaging subsequence embeddings within a recording (i.e., forming a centroid embedding) that the embeddings of each subsequence come from the same distribution. If this assumption holds, then the centroid embedding would approach the central tendency of the subsequence embeddings, leading to improved authentication performance. This assumption is also necessary for the metric learning model to learn a well-clustered embedding space, as the subsequence embeddings for a given subject should follow some central tendency. However, during TEX, for instance, this assumption is certainly violated for whichever subsequence inevitably contains the large return saccade that occurs when a participant finishes reading the text and starts re-reading it. It may be advantageous to exclude such anomalous subsequences, both during training and when forming centroid embeddings.

Third, our impostor pairs always included the first session from one subject and the second session from another subject. As a result, for TEX, reading of the same text was never compared between different subjects. This may have biased the impostor similarities (and by extension our EERs), since we would expect a higher similarity between subjects reading the same text versus different texts. It might be more fair to compare the same session from both subjects when building impostor pairs, similarly to how only the first image of each finger is used for impostor pair generation in [42].

## 6 Conclusion

We presented a metric learning approach for end-to-end biometric authentication using eye movements. Our approach was validated on the GazeBase dataset [14] using recordings collected as much as 37 months apart, and we compared our approach against a statistical baseline. We achieved an EER as low as 3.04% using the full duration (101 seconds) of the horizontal saccades task (HSS), and a FRR @ FAR  $10^{-4}$  as low as 36% using the full duration (60 seconds) of the reading task (TEX). When using only the first window of data (where window size was determined during hyperparameter tuning), we achieved an EER as low as 6.84% and a FRR @ FAR  $10^{-4}$  of 68% using the first 8 seconds of HSS. Since the test set consists of 14 subjects recorded 18 times each over a 37-month period, our results show that eye movement biometrics may be quite resilient against template aging, even when using low-cognitive-load tasks. But we are still a far cry from 5% FRR @ FAR  $10^{-4}$ .

We also achieved an EER as low as 5.68% after downsampling eye movement signals during reading from 1000 Hz to 50 Hz. But the corresponding FRR @ FAR  $10^{-4}$  was 96%, indicating that the system would be unusable in practice.

We believe that the scope and diversity (not only in terms of tasks, but also participant characteristics) of the GazeBase dataset gives it potential to serve as a unifying dataset for future biometrics research. We also encourage future eye

movement biometrics studies to report FRR @ FAR  $10^{-4}$  in a combined effort to eventually achieve the FIDO Alliance's recommendation of 5% FRR @ FAR  $10^{-4}$ .

## Acknowledgment

The authors would like to thank Dr. Lee Friedman for his help with the statistical analysis of our results in SAS. This material is based upon work supported by the National Science Foundation Graduate Research Fellowship under Grant No. DGE-1144466. The study was also funded by 3 grants to Dr. Komogortsev: (1) National Science Foundation, CNS-1250718 and CNS-1714623, [www.NSF.gov](http://www.NSF.gov); (2) National Institute of Standards and Technology, 60NANB15D325, [www.NIST.gov](http://www.NIST.gov); (3) National Institute of Standards and Technology, 60NANB16D293. Any opinions, findings, and conclusions or recommendations expressed in this material are those of the author(s) and do not necessarily reflect the views of the National Science Foundation or the National Institute of Standards and Technology.

## References

- [1] Christina Katsini, Yasmeen Abdrabou, George E. Raptis, Mohamed Khamis, and Florian Alt. The Role of Eye Gaze in Security and Privacy Applications: Survey and Future HCI Research Directions. In *Proceedings of the 2020 CHI Conference on Human Factors in Computing Systems*, CHI '20, pages 1–21, Honolulu, HI, USA, April 2020. Association for Computing Machinery.
- [2] Gary Bargary, Jenny M. Bosten, Patrick T. Goodbourn, Adam J. Lawrance-Owen, Ruth E. Hogg, and J. D. Mollon. Individual differences in human eye movements: An oculomotor signature? *Vision Research*, 141:157–169, December 2017.
- [3] O. V. Komogortsev, A. Karpov, and C. D. Holland. Attack of mechanical replicas: Liveness detection with eye movements. *IEEE Transactions on Information Forensics and Security*, 10(4):716–725, 2015.
- [4] S. Makowski, L. A. Jäger, P. Prasse, and T. Scheffer. Biometric identification and presentation-attack detection using micro- and macro-movements of the eyes. In *2020 IEEE International Joint Conference on Biometrics (IJCB)*, pages 1–10, 2020.
- [5] Simon Eberz, K. Rasmussen, Vincent Lenders, and Ivan Martinovic. Preventing lunchtime attacks: Fighting insider threats with eye movement biometrics. 2015.
- [6] Pawel Kasprowski and Katarzyna Harezlak. Fusion of eye movement and mouse dynamics for reliable behavioral biometrics. *Pattern Analysis and Applications*, 21(1):91–103, February 2018.
- [7] Florian Schroff, Dmitry Kalenichenko, and James Philbin. FaceNet: A unified embedding for face recognition and clustering. In *Proceedings of the IEEE Computer Society Conference on Computer Vision and Pattern Recognition*, volume 07-12-June-2015, pages 815–823. IEEE Computer Society, oct 2015.
- [8] H. B. Kashani, S. Reza, and I. S. Rezaei. On metric-based deep embedding learning for text-independent speaker verification. In *2020 6th Iranian Conference on Signal Processing and Intelligent Systems (ICSPIS)*, pages 1–7, 2020.
- [9] Malik Boudiaf, Jérôme Rony, Imtiaz Masud Ziko, Eric Granger, Marco Pedersoli, Pablo Piantanida, and Ismail Ben Ayed. A unifying mutual information view of metric learning: Cross-entropy vs. pairwise losses. In Andrea Vedaldi, Horst Bischof, Thomas Brox, and Jan-Michael Frahm, editors, *Computer Vision – ECCV 2020*, pages 548–564, Cham, 2020. Springer International Publishing.
- [10] X. Wang, X. Han, W. Huang, D. Dong, and M. R. Scott. Multi-similarity loss with general pair weighting for deep metric learning. In *2019 IEEE/CVF Conference on Computer Vision and Pattern Recognition (CVPR)*, pages 5017–5025, 2019.
- [11] Mahmut Kaya and Hasan Şakir Bilge. Deep metric learning: A survey. *Symmetry*, 11(9):1066, aug 2019.
- [12] Ahmed Abdelwahab and Niels Landwehr. Deep Distributional Sequence Embeddings Based on a Wasserstein Loss. *arXiv:1912.01933 [cs, stat]*, December 2019. arXiv: 1912.01933.
- [13] Dillon J Lohr, Samantha Aziz, and Oleg Komogortsev. Eye movement biometrics using a new dataset collected in virtual reality. In *ACM Symposium on Eye Tracking Research and Applications*, ETRA '20 Adjunct, New York, NY, USA, 2020. Association for Computing Machinery.
- [14] Henry Griffith, Dillon Lohr, Evgeny Abdulin, and Oleg Komogortsev. Gazebase: A large-scale, multi-stimulus, longitudinal eye movement dataset, 2020.



- [15] C. Holland and O. V. Komogortsev. Biometric identification via eye movement scanpaths in reading. In *2011 International Joint Conference on Biometrics (IJCB)*, pages 1–8, 2011.
- [16] Chunyong Li, Jiguo Xue, Cheng Quan, Jingwei Yue, and Chenggang Zhang. Biometric recognition via texture features of eye movement trajectories in a visual searching task. *PLoS ONE*, 13(4):e0194475, apr 2018.
- [17] Paweł Kasprowski and Józef Ober. Eye movements in biometrics. *Lecture Notes in Computer Science (including subseries Lecture Notes in Artificial Intelligence and Lecture Notes in Bioinformatics)*, 3087:248–258, 2004.
- [18] Chiara Galdi, Michele Nappi, Daniel Riccio, and Harry Wechsler. Eye movement analysis for human authentication: a critical survey. 84:272–283.
- [19] Ioannis Rigas and Oleg V. Komogortsev. Current research in eye movement biometrics: An analysis based on BioEye 2015 competition. 58:129–141.
- [20] Richard Andersson, Linnea Larsson, Kenneth Holmqvist, Martin Stridh, and Marcus Nyström. One algorithm to rule them all? An evaluation and discussion of ten eye movement event-detection algorithms. *Behavior Research Methods*, 49(2):616–637, 2017.
- [21] Shaohua Jia, Do Hyong Koh, Amanda Seccia, Pasha Antonenko, Richard Lamb, Andreas Keil, Matthew Schneps, and Marc Pomplun. Biometric recognition through eye movements using a recurrent neural network. In *Proceedings - 9th IEEE International Conference on Big Knowledge, ICBK 2018*, pages 57–64. Institute of Electrical and Electronics Engineers Inc., dec 2018.
- [22] Anjith George and Aurobinda Routray. A score level fusion method for eye movement biometrics. *Pattern Recognition Letters*, 82:207–215, oct 2016.
- [23] Henry K. Griffith and Oleg V. Komogortsev. Texture feature extraction from free-viewing scan paths using gabor filters with downsampling. In *ACM Symposium on Eye Tracking Research and Applications, ETRA '20 Adjunct*, pages 1–3. Association for Computing Machinery.
- [24] Lee Friedman, Mark S. Nixon, and Oleg V. Komogortsev. Method to assess the temporal persistence of potential biometric features: Application to oculomotor, gait, face and brain structure databases. *PLoS ONE*, 12(6):1–42, 06 2017.
- [25] Lee Friedman, Ioannis Rigas, Evgeny Abdulin, and Oleg V. Komogortsev. A novel evaluation of two related and two independent algorithms for eye movement classification during reading. *Behavior Research Methods*, 50(4):1374–1397, 08 2018.
- [26] Ioannis Rigas, Lee Friedman, and Oleg Komogortsev. Study of an extensive set of eye movement features: Extraction methods and statistical analysis. *Journal of Eye Movement Research*, 11(1), 2018.
- [27] Parag K. Mital, Tim J. Smith, Robin L. Hill, and John M. Henderson. Clustering of gaze during dynamic scene viewing is predicted by motion. 3(1):5–24.
- [28] Lena A. Jäger, Silvia Makowski, Paul Prasse, Sascha Liehr, Maximilian Seidler, and Tobias Scheffer. Deep eyedentification: Biometric identification using micro-movements of the eye. In Ulf Brefeld, Elisa Fromont, Andreas Hotho, Arno Knobbe, Marloes Maathuis, and Céline Robardet, editors, *Machine Learning and Knowledge Discovery in Databases*, pages 299–314, Cham, 2020. Springer International Publishing.
- [29] Silvia Makowski, Lena A. Jäger, Ahmed Abdelwahab, Niels Landwehr, and Tobias Scheffer. A discriminative model for identifying readers and assessing text comprehension from eye movements. In *Joint European Conference on Machine Learning and Knowledge Discovery in Databases*, pages 209–225. Springer.
- [30] Henry Griffith, Dillon Lohr, and Oleg V. Komogortsev. Gazebase data repository. 9 2020.
- [31] Dillon J. Lohr, Lee Friedman, and Oleg V. Komogortsev. Evaluating the data quality of eye tracking signals from a virtual reality system: Case study using smi’s eye-tracking htc vive, 2019.
- [32] Magic Leap 1. <https://www.magicleap.com/en-us/magic-leap-1>. Accessed: 2021-04-07.
- [33] Vive Pro Eye. <https://www.vive.com/us/product/vive-pro-eye/overview/>. Accessed: 2021-04-07.
- [34] Kevin Musgrave, Serge Belongie, and Ser-Nam Lim. A metric learning reality check. In Andrea Vedaldi, Horst Bischof, Thomas Brox, and Jan-Michael Frahm, editors, *Computer Vision – ECCV 2020*, pages 681–699, Cham, 2020. Springer International Publishing.
- [35] Alexander Hermans, Lucas Beyersdorff, and Bastian Leibe. In Defense of the Triplet Loss for Person Re-Identification. mar 2017.
- [36] R. Hadsell, S. Chopra, and Y. LeCun. Dimensionality reduction by learning an invariant mapping. In *2006 IEEE Computer Society Conference on Computer Vision and Pattern Recognition (CVPR’06)*, volume 2, pages 1735–1742, 2006.

- [37] James Bergstra and Yoshua Bengio. Random search for hyper-parameter optimization. *Journal of Machine Learning Research*, 13(10):281–305, 2012.
- [38] Ilya Loshchilov and Frank Hutter. Decoupled weight decay regularization. In *7th International Conference on Learning Representations, ICLR 2019*. International Conference on Learning Representations, ICLR, nov 2019.
- [39] Kevin Musgrave, Serge Belongie, and Ser-Nam Lim. Pytorch metric learning, 2020.
- [40] Lee Friedman, Hal S Stern, Vladyslav Prokopenko, Shagen Djanian, Henry K. Griffith, and Oleg V. Komogortsev. Biometric performance as a function of gallery size, 2020.
- [41] Stephanie Schuckers, Greg Cannon, and Nils Tekampe. FIDO biometrics requirements. <https://fidoalliance.org/specs/biometric/requirements/>. Accessed: 2021-04-04.
- [42] R. Cappelli, D. Maio, D. Maltoni, J. L. Wayman, and A. K. Jain. Performance evaluation of fingerprint verification systems. *IEEE Transactions on Pattern Analysis and Machine Intelligence*, 28(1):3–18, 2006.
- [43] Ahmed Abdelwahab, Reinhold Kliegl, and Niels Landwehr. A semiparametric model for Bayesian reader identification. In *Proceedings of the 2016 Conference on Empirical Methods in Natural Language Processing*, pages 585–594, Austin, Texas, November 2016. Association for Computational Linguistics.
- [44] Ivo Služanović, Marc Roeschlin, Kasper B. Rasmussen, and Ivan Martinović. Using reflexive eye movements for fast challenge-response authentication. In *Proceedings of the 2016 ACM SIGSAC Conference on Computer and Communications Security, CCS '16*, page 1056–1067, New York, NY, USA, 2016. Association for Computing Machinery.